Symmetry modes, competing interactions, and universal description for modulated phases in the dielectric A_2BX_4 family

Z. Y. Chen* and M. B. Walker
Department of Physics, University of Toronto, Toronto, Ontario, Canada M5S 1A7
(Received 31 August 1990)

A symmetry-based phenomenological model for the modulated structures in the dielectric A_2BX_4 family is constructed. The A_2BX_4 crystals are viewed as layered structures, and the important variables of our model are the amplitudes of two of the single-layer symmetry modes. The free energy is written in terms of the amplitudes of these two symmetry modes, and is found to contain a competing interaction mechanism, which produces a rich phase diagram. The model gives a universal prediction for both the space groups and the modulation wave vectors for the sequences of phase transitions observed experimentally in the entire A_2BX_4 family.
MS code no. BV4402 1990 PACS number(s): 64.60.−i, 64.70.−p, 77.80.Bh

I. INTRODUCTION

Work in recent years has produced much detailed information on the commensurate and incommensurate structures of the K_2SeO_4-type dielectric crystals, commonly called the A_2BX_4 family.[1,2] This family contains a large group of dielectric isostructural crystals having normal-phase space group $Pcmn$ (D_{2h}^{16}). The symbol A in the chemical formula A_2BX_4 represents K^+, Rb^+, Cs^+ or an equivalent monovalent complex such as NH_4^+ and $N(CH_3)_4^+$ (we use TMA to denote $[N(CH_3)_4]_2$ in this paper). The symbol BX_4 represents a divalent tetrahedral complex such as SeO_4^{-2}, $ZnCl_4^{-2}$, or $ZnBr_4^{-2}$. At low temperatures, a variety of structure-modulated phases, with wave vectors along the orthorhombic c^* direction, have been discovered; these phases have been recently reviewed by Cummins.[2] For example, the prototypical crystal K_2SeO_4 exhibits an incommensurate phase below 130 K with a wave vector close to $c^*/3$ and undergoes a lock-in transition at 93 K to a phase having a wave vector $c^*/3$.[3−5] In other materials, the sequences of the phases and the corresponding wave vectors are somewhat different. For example, in the case of Rb_2ZnBr_4, a commensurate phase with a wave vector $5c^*/17$ is believed to exist between the incommensurate and the commensurate $c^*/3$ states;[6,7] furthermore, there exists in this material a transition between two commensurate phases having different space-group symmetries but both corresponding to wave vector $c^*/3$. As another example, in the case of TMA·$CoCl_4$, a sequence of modulated phases is observed which has wave vectors $(\frac{2}{5}+\delta)c^*$, $\frac{2}{5}c^*$, $(\frac{2}{5}-\delta)c^*$, and $\frac{1}{3}c^*$, corresponding to incommensurate, commensurate, incommensurate, and commensurate phases, respectively (in the order of decreasing temperature).[8−10]

Landau-type theories represent one of the two main types of theories that have been used to understand the different incommensurate and commensurate phases which occur in the A_2BX_4 family.[11,12] For example, Iizumi *et al.*[3] established a model for the lockin to the $c^*/3$ commensurate phase which occurs in potassium selenate by including a term in the free energy coupling the ferroelectric polarization to the cube of the primary order parameter; since the ferroelectric polarization is cubic in the primary order parameter, this coupling term is effectively of sixth order in the primary order parameter (see also Ishibashi, Ref. 12). This work was extended by Mashiyama *et al.*[13] to include the couplings of the primary order parameter to secondary order parameters which were appropriate to account for the $2c^*/5$ phase. Marion *et al.*[14] then introduced the terms in the free energy which were needed to stabilize the $3c^*/7$ phase. Finally, Parlinski and Dénoyer[15] gave a general prescription for finding the terms in the free energy necessary to stabilize a commensurate phase characterized by wave vector nc^*/m. The advantages of these Landau-type theories[3,12−15] are that they are symmetry based and can account for the space-group symmetries of the phases which they have been developed to describe. The major difficulty with these theories, from the point of view of the present paper, is that commensurate phases having distinct wave vectors are stabilized by distinct independent contributions to the free energy, and for materials exhibiting different sequences of phases, different theoretical models therefore are needed.

Yamada and Hamaya[16] made an interesting attempt to construct a unified picture for the modulated phases occurring in the entire A_2BX_4 family. Their extended ANNNI (axial next-nearest-neighbor Ising) model[17] produces sequences of incommensurate and commensurate phases which they used to explain the sequences of phase transitions experimentally found in some crystals in the A_2BX_4 family. Also, they suggested that the Ising spin variable in their model should be identified with a particular local vibration of the A_2BX_4 structure. However, they did not characterize the local vibration in terms of its symmetry so that the identification of the space-group symmetries of the various commensurate phases was beyond the scope of their approach, as was the possibility of considering transitions between two phases of different symmetries corresponding to the same commensurate wave vector.

Our approach depends on identifying appropriate local vibrational variables in terms of which a model free energy can be constructed. The A_2BX_4 crystals are viewed as layered structures, and the possible ionic-distortion modes of an isolated layer are classified according to their symmetries. We then make use of the fact that the three-dimensional distortion modes which give rise to the modulated structures (e.g., the soft mode observed in K_2SeO_4)[3] have a known symmetry. Two (and only two) of the layer modes can produce distortions which give three-dimensional modes of the correct symmetry, and it is therefore necessary to take the amplitudes of these *two* layer modes as the variables in terms of which our model is formulated. Since the symmetries of these two local variables are known, the space-group symmetries of any modulated structure predicted by the model can be found.

As just mentioned, our model contains two distinct symmetry modes per layer. The model free energy contains interactions between nearest-neighbor layer modes of the same symmetry, as well as an interaction which couples nearest-neighbor layer modes of different symmetries. These two different types of interactions favor ground states of different periods. Hence, our model is a competing interaction type of model. However, the model is different from the ANNNI-type competing interaction models in that the competition results from different types of nearest-neighbor interactions,[16–19] rather than from a competition of nearest-neighbor and higher-neighbor interactions.

Janssen[18] has shown that the Janssen-Tjon model[19] (in which the distortion of each layer is characterized by a single variable) can account for some of the observed modulated phases of the A_2BX_4 family. In this approach, the stable commensurate phase of a given wave vector has a unique space-group symmetry, however, whereas more than one space-group symmetry per wave vector has been found to occur experimentally.

Finally, it should be noted that the existence of two interacting modes as a mechanism for the formation of incommensurate structures has been generally discussed previously in a number of contexts.[20–24] However, the discussion has always been carried out in a momentum space framework and has not led to the complex phase diagrams which are characteristic of our local layer-mode, competing-interaction type of approach.

In this paper, we present a detailed derivation and analysis of our model. In Secs. II A and II B, a symmetry analysis is presented and the free energy is constructed. The dispersion curves that determine the incommensurate instability for the high-temperature normal phase are derived in Sec. II C. Our numerical procedure and the results for the phase diagrams are discussed in Sec. III. Since our model is based on a symmetry analysis, we are above to relate the basic variables in our model to symmetry modes for the A_2BX_4 family. Consequently, we can predict space-group symmetries for different modulated phases resulting from our model. Our results are compared with the experimentally determined structures in the A_2BX_4 family in Sec. IV. Some preliminary results were reported in a Letter.[25]

II. FREE ENERGY

A. Symmetry analysis

The crystallographic setting used in this paper to describe the high-temperature (unmodulated) structure of A_2BX_4-type crystals is illustrated in Fig. 1. The unit cell contains four formula units, and the structure can be viewed as being made up of layers which are equidistant and perpendicular to the c axis. The space group of this structure, which is $Pcmn(D_{2h}^{16})$, can be generated by the symmetry elements $\{\sigma_x|\frac{1}{2}0\frac{1}{2}\}$, $\{\sigma_y|0\frac{1}{2}0\}$, and $\{\sigma_z|\frac{1}{2}\frac{1}{2}0\}$; in writing these symmetry elements, the origin is assumed to lie in one of the layers, and is centered in the rectangular basal-plane unit cell shown in Fig. 1.

For the crystals of interest in this article, the modulation wave vector $\mathbf{k}=(0,0,\alpha c^*)$ lies along the c direction (here $c^*=2\pi/c$). Iizumi *et al.* have analyzed the symmetry-mode displacements of wave vector $\mathbf{k}$ for K_2SeO_4.[3] [Symmetry modes are those displacements that transform like the basis vectors of a particular irreducible representation (IRREP) of the space group.] The Iiziumi *et al.* analysis was subsequently widely used for the entire A_2BX_4 family.

Here we present a different approach to the symmetry analysis. The symmetry modes of the individual layers of the A_2BX_4 structure are first determined, and the various three-dimensional modulated structure in the A_2BX_4 family are described in terms of the symmetry modes associated with the different layers.

The space group describing the symmetry of an isolated layer of the A_2BX_4 structure (see Fig. 1) is generated

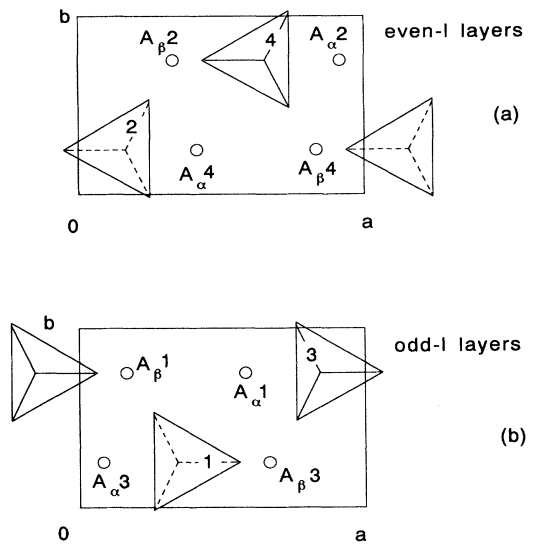

FIG. 1. The structure of A_2BX_4 at its normal phase projected along the c axis. The structure is shown here with two layers at $z=\frac{1}{4}c$ and $\frac{3}{4}c$. Each layer contains two formula units. All four tetrahedra are symmetry related and the A ions with the same Greek subscripts are symmetry related also. Each layer has a three-dimensional structure which is hown here by the projections of ions onto that layer.

TABLE I. The character table of the irreducible representations (IRREP's) of C_{2v}. The group E, C_{2x}, σ_y, σ_z, and IRREP's Γ_i $(i=1,2,3,4)$ are for layer modes; the group E, C_{2z}, σ_y, σ_x, and IRREP's Λ_i $(i=1,2,3,4)$ are for three-dimensional modes.

	E	C_{2x}	σ_y	σ_z	
Γ_1	1	1	1	1	Λ_1
Γ_2	1	1	−1	−1	Λ_2
Γ_3	1	−1	−1	1	Λ_3
Γ_4	1	−1	1	−1	Λ_4
	E	C_{2z}	σ_y	σ_x	

by the symmetry elements $\{\sigma_y|0\frac{1}{2}\}$, $\{\sigma_z|\frac{1}{2}\frac{1}{2}\}$, and $\{C_{2x}|\frac{1}{2}0\}$. Since there is no modulation in the direction perpendicular to the c^* axis, we consider here only zone-center modes for a layer, i.e., modes for which the relative ion displacements in any one unit cell of the layer are identical to those in any other. The little cogroup for the zone-center wave vector is C_{2v}, and its irreducible representations are listed in Table I. Only the modes of symmetry Γ_2 and Γ_3 are of interest in this paper (see below) and these modes are illustrated pictorially in Figs. 2 and 3. Following Iizumi *et al.*,[3] the BX_4 tetrahedra are assumed to move rigidly, and the internal degrees of freedom are neglected. The movements of the BX_4 tetrahedra in the Γ_2 and Γ_3 modes are therefore characterized by giving their rotations about the a and c directions, and their displacements in the b direction. In addition, to completely describe the Γ_2 and Γ_3 modes, the b-axis displacements of the four A ions in the layer unit cell must be specified. Thus, a total of ten quantities (of which five are independent) must be given to specify the Γ_2 or Γ_3 model of a layer. This can be done in terms of ten-component basis vectors, called $e_l(\Gamma_2)$ and $e_l(\Gamma_3)$, for layer l where l is an integer.

The symmetry properties of the modes illustrated in Fig. 2 can be obtained by inspection. For example, the Γ_2 modes satisfy

$$\begin{aligned}&\{C_{2x}|\tfrac{1}{2}00\}e_l(\Gamma_2)=e_{-l}(\Gamma_2)\ ,\\ &\{\sigma_y|0\tfrac{1}{2}0\}e_l(\Gamma_2)=-e_l(\Gamma_2)\ ,\\ &\{\sigma_z|\tfrac{1}{2}\tfrac{1}{2}0\}e_l(\Gamma_2)=-e_{-l}(\Gamma_2)\ ,\end{aligned}\tag{2.1}$$

whereas the Γ_3 modes satisfy

$$\begin{aligned}&\{C_{2x}|\tfrac{1}{2}00\}e_l(\Gamma_3)=-e_{-l}(\Gamma_3)\ ,\\ &\{\sigma_y|0\tfrac{1}{2}0\}e_l(\Gamma_3)=-e_l(\Gamma_3)\ ,\\ &\{\sigma_z|\tfrac{1}{2}\tfrac{1}{2}0\}e_l(\Gamma_3)=e_{-l}(\Gamma_3)\ .\end{aligned}\tag{2.2}$$

For the layer $l=0$, these results, when compared with Table I, confirm the fact that the layer modes labeled by Γ_2 or Γ_3 indeed transform according to these representations. In addition, these modes obey

$$\begin{aligned}&\{C_{2z}|\tfrac{1}{2}\tfrac{1}{2}\tfrac{1}{2}\}e_l(\Gamma_j)=-e_{l+1}(\Gamma_j)\ ,\\ &\{\sigma_y|0\tfrac{1}{2}0\}e_l(\Gamma_j)=-e_l(\Gamma_j)\ ,\\ &\{\sigma_x|\tfrac{1}{2}0\tfrac{1}{2}\}e_l(\Gamma_j)=e_{l+1}(\Gamma_j)\ ,\end{aligned}\tag{2.3}$$

where $j=2,3$.

To find out the relationship between the layer modes the three-dimensional modes, Bloch functions corresponding to an extended-zone c-axis wave vector k can be formed using

$$e_k^j=\sum_l e^{ikz_l}e_l(\Gamma_j)\ ,\tag{2.4}$$

where $z_l=lc/2$ and $j=2,3$. The character table of the

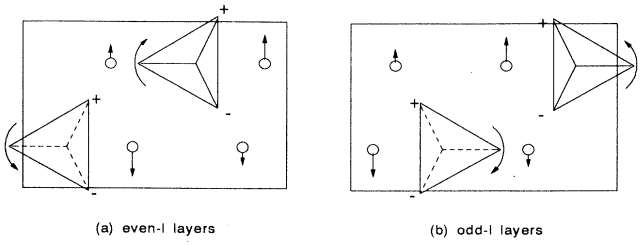

FIG. 2. The ion displacements in the single-layer modes of Γ_2 symmetry for (a) even-l layers and (b) odd-l layers. The two A_α ions in the layer unit cell have b-axis displacements of equal magnitude but opposite direction, as do the two A_β ions and the two BX_4 tetrahedra. The displacements of the A_α and A_β ions are indicated by arrows but, for simplicity, the displacements of the BX_4 tetrahedra are not shown. The two BX_4 tetrahedra in the layer unit cell undergo rotations about the c axis of equal magnitude and opposite directions as indicated by the arcs with attached arrows. The two tetrahedra also undergo rotations about the a axis which are of the same magnitude and direction; the direction of the a-axis rotation is indicated by putting a plus sign (or minus sign) next to the corner of the tetrahedron which is displaced in the positive (or negative) c direction. The locations of the A_α and A_β are as identified in Fig. 1.

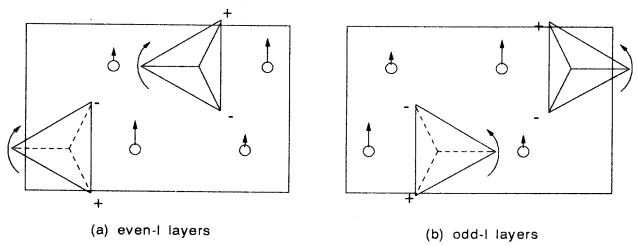

FIG. 3. The ion displacements in the single-layer modes of Γ_3 symmetry for (a) even-l layers and (b) odd-l layers. The two A_α ions in the layer unit cell have b-axis displacements of equal magnitude and direction, as do the two A_β ions and the two BX_4 tetrahedra. The two BX_4 tetrahedra in the layer unit cell also have c-axis rotations having equal magnitudes and directions, and a-axis rotations having equal magnitudes but opposite directions.

little cogroup of the wave k (which contains the elements E, C_{2z}, σ_y, and σ_x) is given in Table I. By using Eq. (2.3), one can show that the Bloch functions in Eq. (2.4) belong to the IRREP Λ_3 if $|k|<\pi/c$. If $\pi/c<|k|<2\pi/c$, the k in Eq. (2.4) should be replaced by the appropriate reduced-zone wave vector k_r by making the substitution $k=c^*-k_r$; these modes can then be shown to transform according to the IREEP Λ_2 of Table I. It is the three-dimensional Λ_2 and Λ_3 modes which are found experimentally to be the soft modes which are responsible for the modulated structures occurring in the A_2BX_4 family.[1] Equation (2.4) shows how the Γ_2 and Γ_3 layer modes can be superposed to give three dimensional Λ_2 and Λ_3 modes. Furthermore, it can be shown that the Γ_1 and Γ_4 layer modes cannot participate in the Λ_2 and Λ_3 modes (since they will produce ion displacements along the a or c directions, for example). Therefore, in constructing a model of the modulated phases for the A_2BX_4 family in terms of layer variables, it is the variables describing the Γ_2 and Γ_3 layer modes which are appropriate. Experimental studies of the soft mode in K_2SeO_4 indicate that the Γ_2 and Γ_3 contributions are comparable in magnitude, and this gives an experimental basis for including two order parameters per layer as we do. In comparison, Janssen[18] used only one mode (which we interpret to be analogous to our Γ_2 mode) in an attempt to explain the phase-transition sequences in some A_2BX_4 compounds.

B. Free energy and competing interactions

The displacements of the ions of layer l are represented by

$$u_l=v_l e_l(\Gamma_2)+w_l e_l(\Gamma_3) \tag{2.5}$$

where $e_l(\Gamma_2)$ and $e_l(\Gamma_3)$ are the normalized basis vector for the symmetry modes defined in Figs. 2 and 3. The variables v_l and w_l are real, and are the amplitudes of the Γ_2 and Γ_3 modes for layer l.

The free energy, which is invariant under the transformations of the space group *Pcmn*, [e.g., the transformations of Eqs. (2.1)–(2.3)], is written as

$$\begin{aligned}F=&\sum_l\left(\tfrac{1}{2}av_l^2+\tfrac{1}{4}v_l^4+\tfrac{1}{2}a'w_l^2+\tfrac{1}{4}w_l^4+\tfrac{1}{2}\gamma v_l^2w_l^2\right)\\&+\sum_l\left[\frac{J}{2}v_lv_{l+1}+\frac{J'}{2}w_lw_{l+1}\right]\\&+\sum_l\left[\tfrac{1}{2}(v_lw_{l+1}-v_{l+1}w_l)\right],\end{aligned} \tag{2.6}$$

where the coefficients of the v_l^4 and w_l^4 terms and of the mixing interaction terms are absorbed into the definitions of the real variables v_l and w_l and the free energy. There are five undetermined coefficients a, a', γ, J, and J' in the free energy (2.6). In a mean-field theory like that of Eq. (2.6), these coefficients can be assumed to be system dependent. For instance, the coefficients a and a' can be assumed linear in temperature and pressure.

We note that although our model has the appearance of a one-dimensional one, it is in fact three dimensional. This is because the v_l and w_l are layer variables. In analyzing the fluctuations, v_l and w_l would have to be considered functions of positions in the layer, i.e., v_l and w_l would vary as one went from one unit cell to another in the layer. These fluctuation effects have been ignored in the present mean-field treatment of the free energy in Eq. (2.6).

In a mean-field theory, the ground state of the free energy (2.6) corresponds to the v_l and w_l profile that produces the lowest free energy. The terms under the first summation produce a typical double-well form for symmetry-breaking phase transitions. This is similar to the Janssen-Tjon model and the mean-field theory of the ANNNI model, which also contain terms having double-well form.[17–19,26] The self-interaction term coupling v_l and v_{l+1} favors a ferromagnetic-type profile $(++++)$ for v_l when $J<0$, or an antiferromagnetic-type profile $(+-+-)$ for v_l when $J>0$, where $+$ and $-$ refer to the signs of the variable v_l. The self-interaction term coupling w_l and w_{l+1} also favors a ferromagnetic- or antiferromagnetic-type profile depending on the sign of the coefficient, similar to the v_lv_{l+1} coupling term. The mixing-interaction term coupling v_l with w_{l+1} and v_l with w_{l-1}, however, favors a four-layer period for v_l of the form $(++--)$, while w_l has the form $(+--+)$. There is thus a competition between the self- and the mixing-interaction terms, although only nearest-neighbor interactions are considered here. This competition is the fundamental mechanism producing the modulated phases in our model; it is different from the mechanism of other competing interactions models, such as the ANNNI model and the Janssen-Tjon model, that rely on an interaction higher than nearest neighbor to produce competing interactions.[16–19]

The low-temperature behavior of (2.6), when $|a|\sim|a'|\gg|J|,1$, can be called the "Ising limit." At this limit, the magnitudes of the variables v_l and w_l are mainly determined by the double-well term in (2.6). For small γ, $v_l=\pm\sqrt{a}\equiv s_l\sqrt{a}$ and $w_l=\pm\sqrt{a'}\equiv t_l\sqrt{a'}$. At this limit, the interaction terms are treated as perturbations to the double-well terms. To first order in the perturbation theory, the free energy is determined by a particular configuration of the spin-$\frac{1}{2}$-like variables s_l and t_l, and becomes that of a one-dimensional, axial nearest-neighbor double Ising model:

$$\begin{aligned}F_I=&\sum_l\left(\tfrac{1}{2}Ja^2s_ls_{l+1}+\tfrac{1}{2}J'a'^2t_lt_{l+1}\right)\\&+\sum_l aa'(s_lt_{l+1}-s_{l+1}t_l)\ .\end{aligned} \tag{2.7}$$

When $J=J'$ and $a=a'$, one can show that there are only three stable phases: a ferromagnetic-type phase with configurations $(++++)$ for both v_l and w_l when $J<-1$, an antiferromagnetic-type phase with $(+-+-)$ for both v_l and w_l when $J>1$, and a four-layer period phase with $(++--)$ for v_l and $(+--+)$ for w_l when $-1<J<1$.

In general, the minimum of the free energy (2.6) cannot be determined analytically. We present in Sec. III a nu-

merical procedure to determine the minima of the free energies corresponding to periodic solutions in v_l and w_l.

C. The stability of the normal phase

In this section, we obtain an expression for the free energy, valid for small displacements of the ions from their normal-phase positions, which is useful in exploring the stability of the normal phase.

Introducing into Eq. (2.6) the Fourier transforms of the variables v_l and w_l,

$$v_l=\sum_k e^{iklc'}\bar{v}_k,\quad w_l=\sum_k e^{iklc'}\bar{w}_k i\ , \tag{2.8}$$

leads to, for the quadratic term of the free energy per layer,

$$f_2=\sum_k(\bar{v}_k\bar{w}_k)^*\begin{bmatrix}A & C/2\\ C/2 & B\end{bmatrix}\begin{bmatrix}\bar{v}_k\\ \bar{w}_k\end{bmatrix}\ , \tag{2.9}$$

where

$$\begin{aligned}A&=\frac{a}{2}+\frac{J}{2}\cos kc'\ ,\\ B&=\frac{a'}{2}+\frac{J'}{2}\cos kc'\ ,\\ C&=-\sin kc'\ .\end{aligned} \tag{2.10}$$

and $c'=c/2$. The expression (2.9) can be further transformed to

$$f_2=\sum_k(\omega_+^2|\Psi_k^+|^2+\omega_-^2|\Psi_k^-|^2)\ , \tag{2.11}$$

where

$$\begin{bmatrix}\Psi_k^+\\ \Psi_k^-\end{bmatrix}=\begin{bmatrix}-\beta & \alpha\\ \alpha & \beta\end{bmatrix}\begin{bmatrix}\bar{v}_k\\ \bar{w}_k\end{bmatrix}\ , \tag{2.12}$$

with coefficients

$$\begin{aligned}\alpha&=\frac{C}{[C^2+4(A-\omega_-^2)^2]^{1/2}}\ ,\\ \beta&=\frac{2(\omega_-^2-A)}{[C^2+4(A-\omega_-^2)^2]^{1/2}}\ .\end{aligned} \tag{2.13}$$

The eigenvalues of the matrix in (2.9) are

$$\omega_\pm^2(k)=\tfrac{1}{2}\{a_+ +J_+\cos kc' \pm[(a_- +J_-\cos kc')^2+\sin^2 kc']^{1/2}\}\ . \tag{2.14}$$

Here we have defined

$$a_\pm=\tfrac{1}{2}(a\pm a'),\quad J_\pm=\tfrac{1}{2}(J\pm J')\ . \tag{2.15}$$

In Eq. (2.14), in spite of the notation, $\omega_\pm^2$ can be either positive or negative. Using Eq (2.3), we can show that the variables $\Psi_k^\pm$ transform like basis vectors for the IRREP Λ_3 when $k<c^*/2$. When $c^*/2<k<c^*$, k is replaced by the reduced-zone wave vector using $k=c^*-k_r$ and the variables $\Psi_k^\pm$ can be shown to transform according to the IRREP Λ_2.

The branch ω_- is always lower than ω_+. The ω_- "dispersion" curve has a minimum at wave vector k_m as shown in Fig. 4. When the temperature is lowered from the normal phase, the minimum of the dispersion curve $\omega_-^2(k)$ goes to zero at the normal-incommensurate transition temperature, and the system undergoes a soft mode, second-order phase transition to a modulated structure with a wave vector k_m which is almost always incommensurate. Just below the normal-incommensurate phase transition, there exists a region in the phase diagram where a phase having the symmetry of the ω_--only mode is stable. The free energy for the ω_--only mode can be compared with the Janssen-Tjon model as in Appendix A. As will be discussed further in Sec. III, when a and a' are lowered, the free energy (2.6) exhibits a second-order phase transition from a phase with the symmetry of the ω_--only mode to a phase with the symmetry of the double ω_--ω_+ mode. This can be seen from expression (2.14); when a_+ is very low, the ω_+ mode also becomes soft.

Finally, we point out an assumption implicit in our model which has not been mentioned above. It is clear from Figs. 2 and 3 that there are three independent translational coordinates and two independent rotational coordinates for both Γ_2 and Γ_3 modes of a single layer. Thus, there are five linearly independent modes for each type of symmetry, Γ_2 and Γ_3. In this paper we assume that it is necessary to consider only *one* Γ_2 mode and *one* Γ_3 mode for each layer (i.e., given bases for the Γ_2 and Γ_3 modes, we consider only one particular linear combination of basis vectors for each layer). However, if the ionic distortions of the normal phase were considered in a more complete way, all of the Γ_2 and Γ_3 modes of a layer would be coupled together, and the particular linear combination of the Γ_2 and Γ_3 layer modes which would be present in a given three-dimensional Λ_2 and Λ_3 mode of wave vector k would vary with wave vector. In the

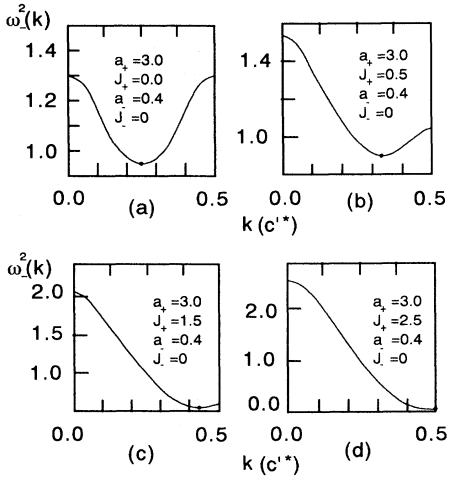

FIG. 4. The dispersion curve for the w_-^2 branch [Eq. (14)]. The minimum in the dispersion curve is emphasized by a dot.

specific cases considered below, the sequences of phases which are found to occur for a given material all have wave vectors close to one another. Thus, we expect our model to be able to predict reasonably well the sequences of phases which occur in any given member of the A_2BX_4 family.

It should be noted that in Fig. 4 there is no acoustic branch of the spectrum,[3] i.e., no branch for which the frequency goes to zero at zero wave vector. This is because we have not assumed that one of the layer modes is a mode in which all ions are given the same displacement. A discussion of phase transitions in which an acoustic mode plays a central role would require an extension of the approach presented here.

III. DESCRIPTION OF THE PHASE DIAGRAMS

A. Numerical procedure

In this section we present the phase diagram for the free energy of Eq. (2.6). Our numerical procedure is similar to that of other competing-interaction models.[17–19] The minimization conditions

$$\frac{\partial F}{\partial v_l}=(a+\gamma\omega_l^2)v_l+v_l^3+\frac{J}{2}(v_{l+1}+v_{l-1}) +\tfrac{1}{2}(w_{l+1}-w_{l-1})=0 , \tag{3.1a}$$

$$\frac{\partial F}{\partial w_l}=(a'+\gamma v_l^2)w_l+w_l^3+\frac{J'}{2}(w_{l+1}+w_{l-1}) +\tfrac{1}{2}(v_{l-1}-v_{l+1})=0 \tag{3.1b}$$

are solved numerically using iteration methods. For solutins with a period m, the boundary conditions $v_{l+m}=v_l$ and $w_{l+m}=w_l$ are imposed, which reduces Eq. (3.1) to a set of $2m$ nonlinear equations. The iteration procedure is as follows. For a given m, initial approximations are chosen before solving the equation. For very large and negative a and a', the analytic solutions of (3.1), i.e., $v_l=0,\pm|a|^{1/2}$ and $w_l=0,\pm|a'|^{1/2}$ are used as initial approximations. All different combinations of these three values for v_l and three values for w_l with periodicity m must be considered. For all other points in the phase diagram, we choose solutions corresponding to a neighboring point, usually of a lower a and a', as initial approximations. At each step of iteration, approximations are used for all variables except v_l in (3.1a) and w_l in (3.1b) for the lth set of equations; if it is the first step, the initial approximations are used, otherwise the results from the previous step are used as the approximations. The roots of the cubic equation (3.1a) in v_l and (3.1b) in w_l are then found, which provide new approximations for the next step.

After the minimization conditions (3.1) are solved for a given m, the free energy per layer F/m is deduced. Minimum free energies for all m are compared to yield the state corresponding to the lowest free energy. If this state has period m and $2n$ nodes per period, the main Fourier component of the profile of v_l and w_l has a wave vector $(n/m)c'^*$ with $c'^*=2\pi/c'$. This phase is therefore labeled by n/m, which is chosen to be irreducible.

We can determine the space-group symmetry from the profile of the variables v_l and w_l using Eqs. (2.1), (2.2), and (2.5). For each phase, we have studied the behavior of the profile of the parameters v_l and w_l. For $n/m=p/(2q+1)$ and $n/m=(2p+1)/2(2q+1)$, where p and q are arbitrary integers that are chosen to make the ratio n/m irreducible, there are three different types of profiles for each wave vector. This yields three different space groups for a given wave vector, as listed in Table II. For $n/m=(2p+1)/4q$, there are only two different types of profiles yielding two different space groups for each wave vector.

Because this procedure yields only commensurate phases, we cannot distinguish between incommensurate states and very-high-order commensurate states. In principle, incommensurate phases should exist just below the normal-incommensurate phase-transition curve (e.g., see Ref. 16). It is common to use superspace groups to describe the space-group symmetry of an incommensurate state.[27] Appendix B is a discussion of the superspace groups of the incommensurate states in the A_2BX_4 family.

TABLE II. Space groups determined from our model for commensurate phases.

n/m	Phases	Space groups	Profile of v_l	Profile of w_l
$n/m=(2p+1)/2(2q+1)$	I	$P112_1/n$	odd in l and even in l-$m/4$	even in l and odd in l-$m/4$
	II	$P2_12_12_1$	even in l and odd in l-$m/4$	odd in l and even in l-$m/4$
	III	$P112_1$	no special symmetry	
$n/m=p/(2q+1)$	I	$Pc2_1n$	odd in l	even in l
	II	$P2_1/c11$	even in l	odd in l
	III	$Pc11$	no special symmetry	
$n/m=(2p+1)/4q$	I	$P12_1/c1$	odd in l-1/2 and even in l-1/2-$m/4$	even in l-1/2 and odd in l-1/2-$m/4$
	II	$P2_1cn$	odd in l and even in l-$m/4$	even in l and odd in l-$m/4$

B. Phase diagrams

As the first example, we take $J_- = \gamma = 0$. The resulting phase diagram is shown in Fig. 5 for an arbitrarily chosen $a_- = 0.4$. At low (i.e., large negative) a_+, the profile of the order parameter implies a structure that has space-group symmetry corresponding to phase III in Table II for wave numbers $n/m = (2p+1)/2(2q+1)$ and $n/m = p/(2q+1)$ and phase I for wave numbers $n/m = (2p+1)/4q$. For wave vector $n/m = (2p+1)/4q$, this symmetry ($P12_1/c1$) remains valid all the way to the normal-incommensurate or normal-commensurate transition line. The phase boundaries between phases having different wave vectors are first order. For wave numbers $n/m = (2p+1)/2(2q+1)$ and $n/m = p/(2q+1)$, there is a phase transition to a phase having the same wave vector but a different space-group symmetry (phase I) when a_+ increases. This phase transition is second order, corresponding to a transition from a phase with the symmetry of a combined ω_+-ω_- mode to a phase with the symmetry of an ω_--only mode. The ω_--only mode is the one that yields the structures which have the most-often-observed symmetry in the A_2BX_4 family. The shaded areas in Fig. 5 represent possible incommensurate and high-order commensurate states.

The second-order phase transition between distinct states having the same wave number can be further studied by evaluating the Fourier spectrum for the profiles of v_l and w_l. For example, the profiles of a $\frac{1}{3}$ phase can be

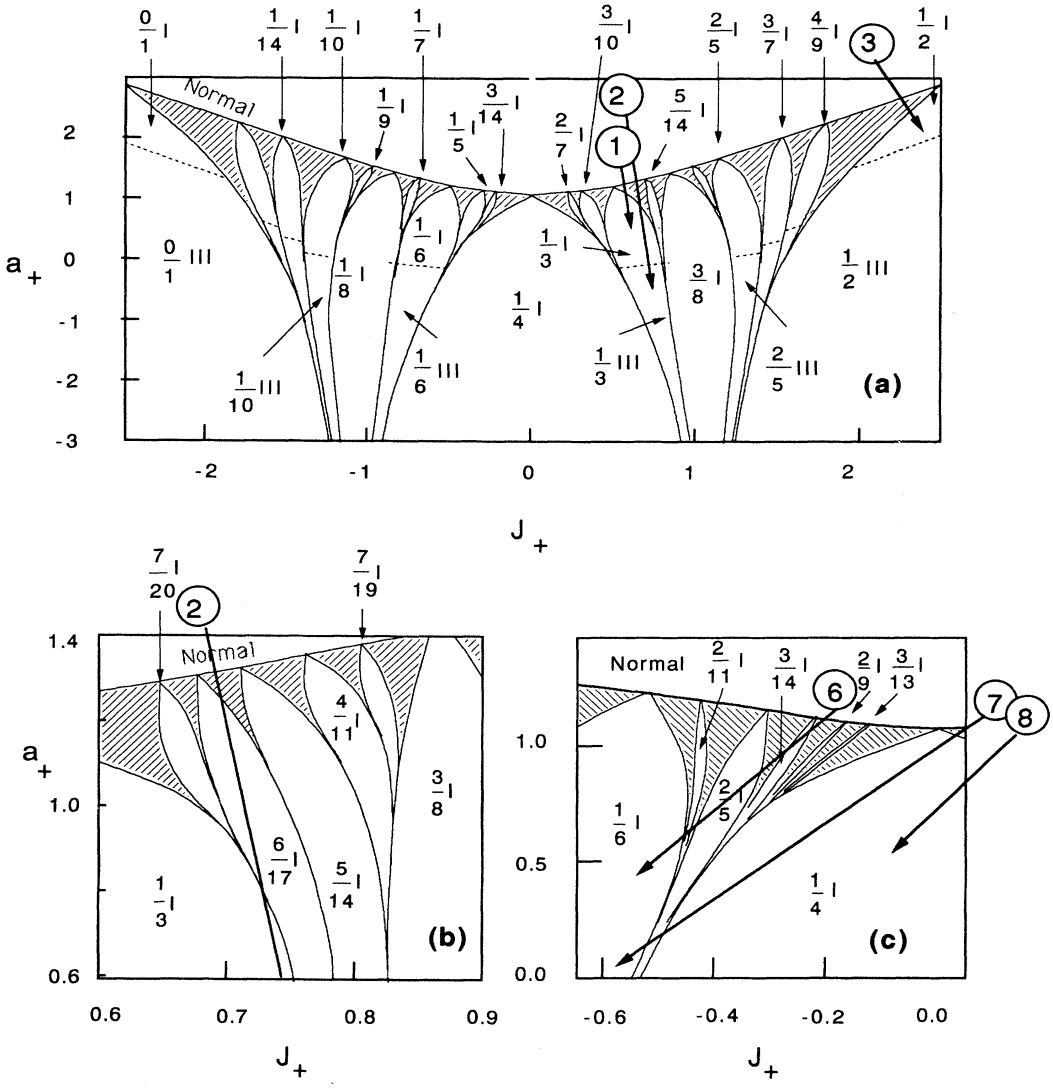

FIG. 5. The phase diagrams produced from our model using $\gamma = 0$, $a_- = 0.4$, and $J_- = 0$. The commensurate phases are labeled by n/m where $(n/m)2\pi/c'$ is the wave vector. The phases are also labeled by the space groups (phase I or III) in Table II. The dashed line represents a second-order phase transition within the same wave vector. The shaded areas indicate higher-order commensurate or incommensurate regions. (a) A global phase diagram with m taken from 1—10. (b) An exploded phase diagram near the $\frac{1}{3}$ phase with m taken from 1–20. (c) An exploded phase diagram near the $\frac{1}{6}$ phase with m taken from 1–15.

decomposed as

$$v_l = C_0 + C_1 \cos\frac{2\pi}{3} l + S_1 \sin\frac{2\pi}{3} l \ , \tag{3.2a}$$

$$w_l = C_0' + C_1' \cos\frac{2\pi}{3} l + S_1' \sin\frac{2\pi}{3} l \ . \tag{3.2b}$$

When $J_+ = 0.5241$, $J_- = 0$, and $a_- = 0.4$, the coefficients C_0, C_1, S_1, C_0', C_1', and S_1' as functions of a_+ are shown in Fig. 6(a). At $a_+ = 1.216$, there is a soft-mode normal-commensurate phase transition to the $\frac{1}{3}$ commensurate phase. For low a_+, there is no obvious symmetry for the profiles of v_l and w_l, and phase III in Table II is valid. When a_+ increases, there is a clear second-order phase transition when the coefficients C_0, C_1, and S_1' vanish, leaving the profile of v_l odd in l and that of w_l even in l. Then phase I in Table II becomes stable.

One interesting aspect of the phase diagram [Fig. 5(a)] is that the phase diagram is symmetric about $J_+ = 0$. When $J_- = 0$, a sign change of J_+ is equivalent to letting all v_l with odd l and all w_l with even l change sign. Counting the number of nodes of the profile v_l and w_l, we conclude that the wave vectors k_- of a stable phase of a $J_+ < 0$ can be deduced from the corresponding wave vector k_+ of the phase at $|J_+|$ using the relationship $k_- = \frac{1}{2}c'^* - k_+$.

In producing Fig. 5, we have arbitrarily chosen $a_- = 0.4$. We note that if one replaces a_- with $-a_-$ the phase diagram in Fig. 5 is not changed but the profiles for v_l and w_l are interchanged, and thus the space group may change when a_- changes sign. In particular, phases with $n/m = p/(2q+1)$ and $n/m = (2p+1)/2(2q+1)$ originally having phase I now have phase II and vice versa; for these wave vectors, the region of stability in Fig. 5 of phase I when $a_- > 0$ and phase II when $a_- < 0$ becomes small when the magnitude of a_- becomes small. When $a_- = 0$, phase I (or II) vanishes, and there is only one possible space group (phase III) for each wave vector. This can also be illustrated using a Fourier spectrum [Fig. 6(b)] for the profile of v_l and w_l for $a_- = 0$ at $J_+ = 1/\sqrt{3}$. All the coefficients vanish at the normal-commensurate transition point. This figure can be compared with the case $a_- = 0.4$ [Fig. 6(a)].

As the second example, we took $a_+ = \gamma = J_- = 0$. The $a_- J_+$ phase diagram is shown in Fig. 7. For a given $n/m = (2p+1)/2(2q+1)$, $n/m = p/(2q+1)$, all three phases in Table II exist. For a given $n_{\text{odd}}/2m_{\text{even}}$, only one phase is stable.

As the third example, we took $J_- = 0$, $J_+ = -0.09$, and $a_- = 0.4$. The stable commensurate phase for low γ is $n/m = \frac{1}{4}$, which has space group $P12_1/c1$. When γ increases, however, there is a first-order phase transition via an intermediate incommensurate phase to a $\frac{1}{4}$ phase with different profiles for v_l and w_l and with the space group $P2_1cn$. This behavior, as shown in Fig. 8(a), is general for all $n/m = (2p+1)/4q$. In the case of $n/m = \frac{3}{8}$, for example, similar phase transitions also exist [Fig. 8(b)].

For wave numbers $n/m = p/(2q+1) > \frac{1}{4}$ and $n/m = (2p+1)/2(2q+1) < \frac{1}{4}$, at sufficient high a_+ with a nonzero a_-, phase I for $a_- > 0$ (or II for $a_0 < 0$) is stable at $\gamma = 0$ as described above. This phase remains stable for low γ, but an increasing γ tends to enlarge the region of stability of phase I (or II). At high γ, phase I (or II) undergoes a first-order phase transition to phase II (or I). However, for $n/m = p/(2q+1) < \frac{1}{4}$ and $n/m = (2p+1)/2(2q+1) > \frac{1}{4}$, such a phase transition does not exist (Fig. 9).

Janssen[18] has also deduced the possible commensurate phase space groups on the basis of symmetry arguments only, and our results are consistent with his considerations. It should be noted, however, that Janssen's analysis of the Janssen-Tjon model[19] finds stable solutions corresponding to only one of the possible space groups for each commensurate wave vector, whereas our model

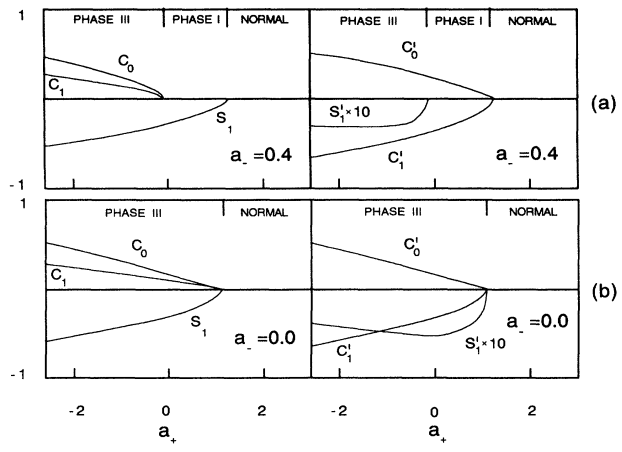

FIG. 6. Fourier spectrum for the profiles of v_l and w_l. Here we use the $\frac{1}{3}$ phase as an example. Please refer to Eq. (3.2) for the definitions of the plotted functions. (a) $J_- = \gamma = 0$, $J_+ = 0.524$, $a_- = 0.4$. (b) $J_- = \gamma = a_- = 0$, $J_+ = 1/\sqrt{3}$.

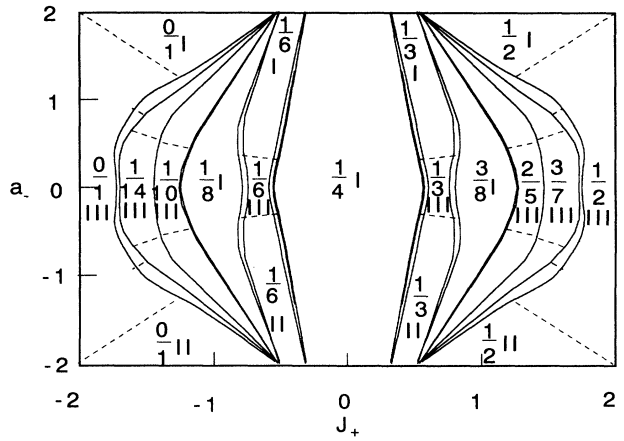

FIG. 7. The phase diagram produced from our model using $a_+ = J_- = \gamma = 0$. The commensurate phases are labeled by n/m where $(n/m)2\pi/c'$ is the wave vector. The phases are also labeled by the space groups (phase I, II, or III) in Table II. The dashed line represents a second-order phase transition within the same wave vector.

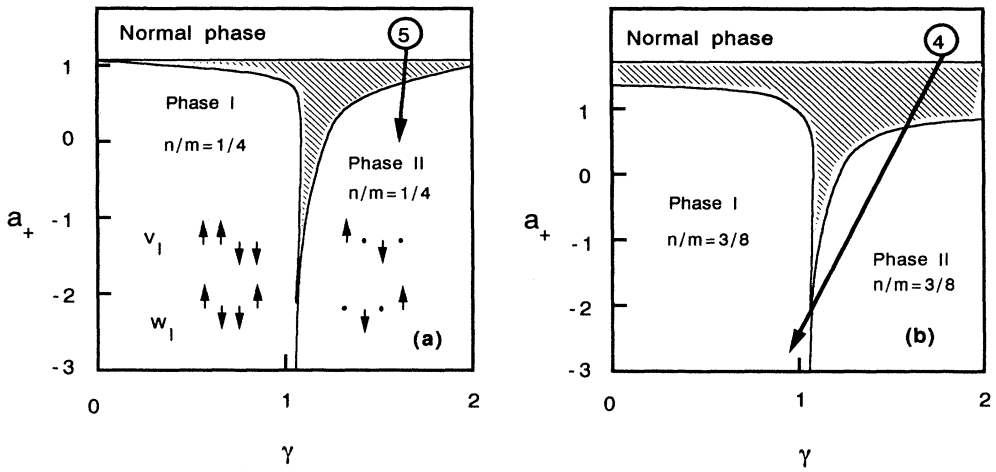

FIG. 8. Phase diagrams for a varying γ with (a) $J_+=-0.09$, $J_-=0$, and $a_-=0.4$. (b) $J_+=0.80$, $J_-=0$, $a_-=0.4$. The shaded area represents incommensurate or high-order commensurate phases. In Fig. 8(a), high-order commensurate phases with wave vectors $n/m=\frac{11}{45},\frac{11}{46},\frac{11}{47}$ are used to determine the phase boundary between the shaded area and the $\frac{1}{4}$ phase. In (b), a high-order commensurate phase with wave vector $\frac{18}{49}$ is used to determine the phase boundary between the shaded area the the $\frac{3}{8}$ commensurate phase.

gives solutions for a wider range of possible space group symmetries, in agreement with experiments.

IV. COMPARISON WITH EXPERIMENTS

The phase diagram developed in this paper, especially space-group symmetries of the stable phases, can be compared with experimental results in the A_2BX_4 family.[28] The commensurate phases in Figs. 5–9 are labeled by n/m, where $k=(n/m)c'^*=(2n/m)c^*$ is the wave vector. Here k corresponds to the extended-zone wave vector of Refs. 1 and 2. The experimentally observed wave vectors of the Λ_2 and Λ_3 modes are usually characterized by the reduced-zone wave vectors $k_r=c^*-k$ and $k_r=k$, respectively. In this section, unless especially specified, wave vectors in mentioned experiments are already converted to the extended-zone scheme. A summary of experimentally observed phases is shown in Fig. 10.

A. The K_2SeO_4 group

The first group of crystals, containing the crystals K_2SeO_4,[3–5] K_2ZnCl_4,[29–32] Rb_2ZnCl_4,[35] Rb_2ZnBr_4,[6,7] and probably Rb_2CoBr_4,[36,37] initially goes through a normal-incommensurate phase transition, and then undergoes an incommensurate-commensurate phase transition. The resultant commensurate phase $n/m=\frac{1}{3}$ has the experimentally determined space group $Pc2_1n$ corresponding to phase I in our model, as in Table II and Fig. 5. We also note that the incommensurate phase is predicted from our model to have superspace group $P^{Pcmn}_{ss\bar{1}}$ (Appendix B). This superspace group is also observed in the crystals K_2SeO_4,[5] K_2ZnCl_4,[29] Rb_2ZnCl_4,[34,35,37] and Rb_2ZnBr_4.[7] In our model, the incommensurate-commensurate phase transitions are first order. This is supported from experimental evidence in K_2SeO_4 and K_2ZnCl_4, that the distortion wave vectors change *discontinuously* across the

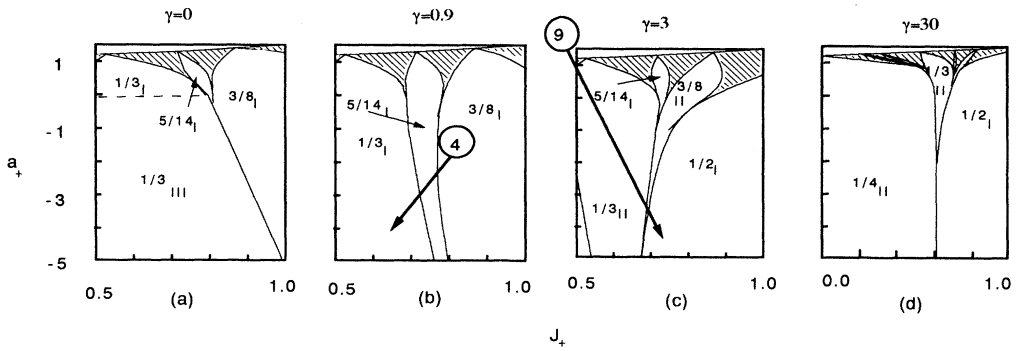

FIG. 9. Phase diagrams for different values of γ: (a) $\gamma=0$, (b) $\gamma=0.9$, (c) $\gamma=3$, and (d) $\gamma=30$. Again, the phases are labeled by the wave numbers n/m and the space groups in Table II. The integer m is taken up to 15.

incommensurate-commensurate phase transition temperatures.[3,30,32] In the crystal Rb_2ZnCl_4, the wave vector seems to change continuously across this phase transition,[32,35] but Mashiyama *et al.* reported that the wave vector is discontinuous on heating.[38] A possible trajectory, labeled by 1, is shown in phase diagram Fig. 5(a) for these crystals.

The crystal Rb_2ZnBr_4 belongs to this group, but an interesting $\frac{6}{17}$ phase is observed between the incommensurate phase and the commensurate $\frac{1}{3}$ phase.[6,7] It has been shown by Randa[39] that in an extended ANNNI model, the $\frac{6}{17}$ phase which was originally shown to appear in the neighborhood of the $\frac{1}{3}$ phase[15] actually does not neighbor the $\frac{1}{3}$ phase. In our model, the $\frac{6}{17}$ phase indeed neighbors the $\frac{1}{3}$ phase, in agreement with the observed behavior of Rb_2ZnBr_4 [see Fig. 5(b)]. The phase transition is first order. The crystal Rb_2ZnBr_4 also displays a sequence of

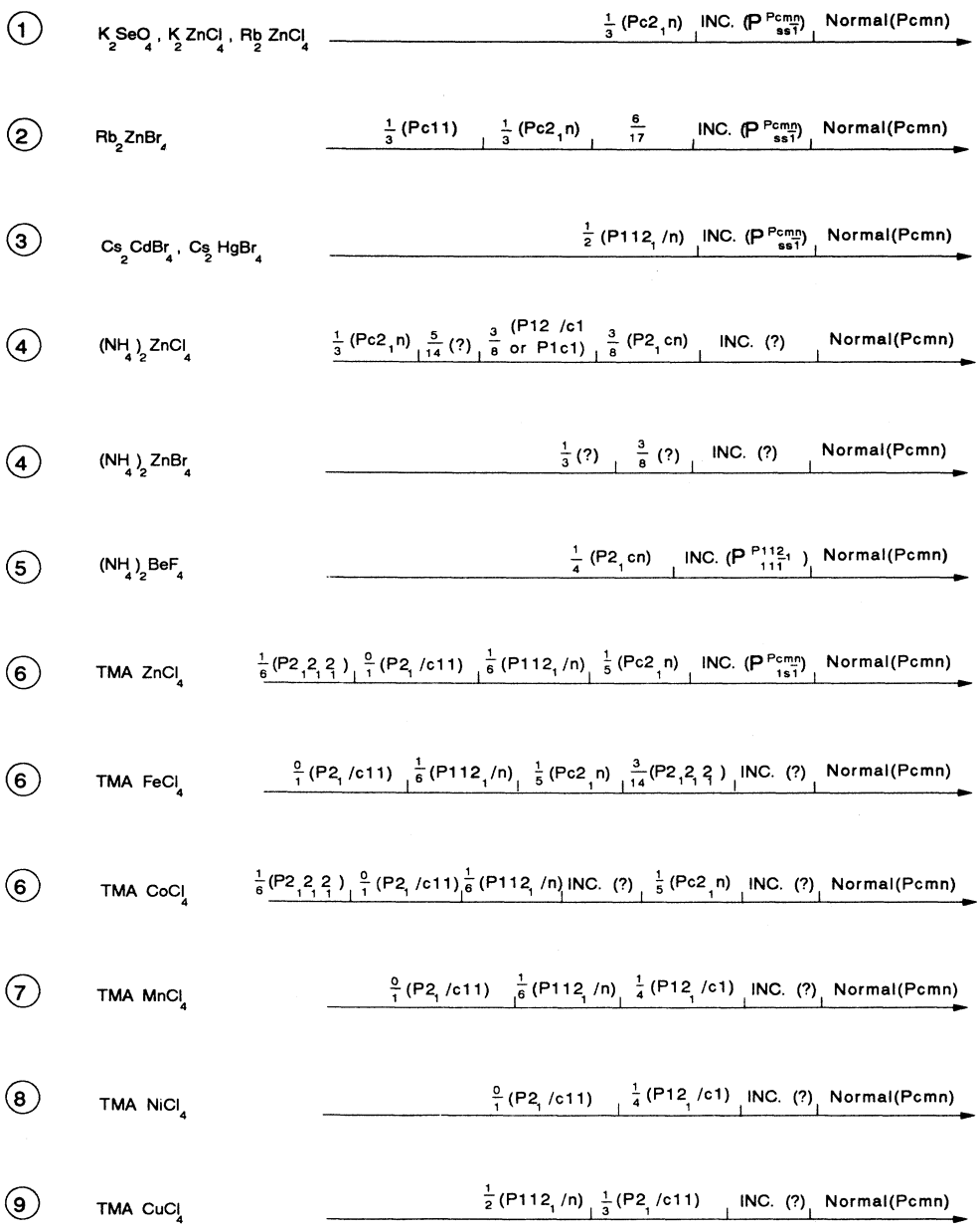

FIG. 10. A summary of modulated phases occurring in the A_2BX_4 family. The integer label in the front of crystal name is the label of trajectory in Figs. 5–9. The fractions n/m are the labels for the commensurate phases, where $k=(n/m)2\pi/c'$ is the wave vector in the extended zone. The Λ_2 and Λ_3 modes are characterized by reduced-zone wave vectors $k_r=c^*-k$ and $k_r=k$, respectively.

phase transitions at low temperatures, including a phase transition from the $\frac{1}{3}(Pc2_1n)$ phase to a $\frac{1}{3}(Pc11)$ phase. This phase transition can be explained by the phase transition from phase I to phase III in our model [see Table II and Fig. 5(a)], which therefore should be second order. This can be supported by the experimental evidence reported by Ueda *et al.*, who measured the intensities of the (050) and (500) reflections as functions of temperature.[40] These reflections vanish *continuously* at the $\frac{1}{3}(Pc2_1n)$-$\frac{1}{3}(Pc11)$ transition temperature, with second order phase-transition characteristics. The specific-heat measurement by Monoto and co-workers[41] shows a swollen specific-heat anomaly, which seems to have the second-order phase-transition characteristics, too. A possible trajectory, labeled by 2, is shown in phase diagram Figs. 5(a) and 5(b) for Rb_2ZnBr_4.

B. The Cs_2CdBr_4 group

The second group is Cs_2CdBr_4 (Refs. 42–44) and Cs_2HgBr_4.[45,46] This group undergoes phase transitions from the normal phase to an incommensurate phase, and then a first-order phase transition to a commensurate phase.[44] This commensurate phase corresponds to the zone-center mode of the IRREP Λ_2, which has $n/m=\frac{1}{2}$ here. The experimentally determined superspace group of the incommensurate phase is $P^{Pcmn}_{ss\bar{1}}$ and the space group for the commensurate phase is $P112_1/n$,[43,44] which is consistent with predictions from our model. A possible trajectory, labeled by 3, is shown in phase diagram Fig. 5(a) for these crystals.

C. The $(NH_4)_2MX_4$ group

The crystal $(NH_4)_2ZnCl_4$ was found by Belobrova *et al.* to be incommensurate.[47] According to the structural analysis by Sato *et al.*,[48] the crystal $(NH_4)_2ZnCl_4$ first goes through a second-order normal-incommensurate phase transition and then a first-order incommensurate-commensurate phase transition to a $\frac{3}{8}$ commensurate phase. Matsunaga[49] determined the space group $P2_1cn$ for this commensurate phase and also discovered a commensurate-commensurate phase transition at a lower temperature to a phase characterized by the same wave vector $\frac{3}{8}$ but with a different space group $P12_1/c1$ or $P1c1$. This commensurate-commensurate phase transition can be explained by Fig. 8(b). The first commensurate phase corresponds to the high-γ phase. If the second one corresponds to the low-γ phase, it should have the space group $P12_1/c1$; however, according to Matsunaga,[49] the structure fits to the space group $P1c1$ with a smaller error. Furthermore, the crystal undergoes a commensurate-commensurate phase transition to the $\frac{1}{3}$ commensurate phase with the space group $Pc2_1n$. This phase transition is also consistent with our model as shown in Fig. 9(b) and Table II. It was reported by Warczewski *et al.*[50] and Sato *et al.*[48] that a $\frac{5}{14}$ phase [or $k_r(\Lambda_2)=\frac{2}{7}c^*$] may coexist with the $\frac{3}{8}$ phase between the $\frac{3}{8}$ and $\frac{1}{3}$ phases in a very narrow temperature range. According to our model, a $\frac{5}{14}$ commensurate phase is possible between these two phases [Fig. 9(b), trajectory 4].

The crystal $(NH_4)_2ZnBr_4$ has a similar wave-vector sequence as $(NH_4)_2ZnCl_4$, but there is only one $\frac{3}{8}$ phase, and the $\frac{5}{14}$ phase does not exist.[51] Structures of the stable phases are not determined experimentally.

The crystal $(NH_4)_2BeF_4$, also denoted as AFB, was discovered by Iizumi and Gesi to have an incommensurate phase.[52] It first undergoes a normal-incommensurate phase transition and then a first-order incommensurate-commensurate phase transition to a $\frac{1}{4}$ phase. Structural analysis performed by Yamada and co-workers[53] indicates that this commensurate phase has the symmetry $P2_1cn$, which can be explained by our model with a high-γ symmetry [Fig. 8(a), trajectory 5]. However, the superspace group for the incommensurate phase determined by Yamada and co-workers is $P^{P112_1}_{11\bar{1}}$ (Yamada and co-workers noted that the basic structure has space group $P112_1$), which is inconsistent with the symmetries of the incommensurate phases in other crystals in the A_2BX_4 family, and is also inconsistent with the prediction of our model.

D. The TMA·MX_4 group

The last group in the A_2BX_4 family consists of a large group of crystals[1,2] commonly denoted TMA·MX_4 (where M=Mn, Fe, Zn, Co, Ni, X=Cl, Br). The modulations in these crystals belong to the IRREP Λ_3 instead of Λ_2 as in other groups. When the temperature is lowered from the normal phase, this group of crystals initially goes through a normal-incommensurate phase transition to an incommensurate phase with various wave vectors. For the incommensurate phase of the crystal TMA·$ZnCl_4$, Madariaga *et al.*[54] have determined superspace group $P^{Pcmn}_{1s\bar{1}}$, which is characteristic for a Λ_3 incommensurate phase as discussed in Appendix B.

Tanisaki and Mashiyama determined the commensurate structures of the crystal TMA·$ZnCl_4$.[55] The first three modulated phases can be characterized by wave vectors and space groups $\frac{1}{5}+\delta$(incommensurate), $\frac{1}{5}(Pc2_1n)$, and $\frac{1}{6}(P112_1/n)$. They also determined the structures of the crystal TMA·$FeCl_4$ which has the sequence of phase[56] $\frac{1}{5}+\delta$(incommensurate) and $\frac{1}{6}(P112_1/n)$. The temperature dependences of modulation wave vector measured by Marion *et al.*[57] for TMA·$ZnCl_4$ and Iizumi and Gesi[58] for *d*-TMA·$ZnCl_4$ indicates that the $\frac{1}{5}+\delta$-incommensurate–$\frac{1}{5}$-commensurate and the $\frac{1}{5}$-commensurate–$\frac{1}{6}$-commensurate phase transitions are first order. Hasabe *et al.*[8] determined the structure of the crystal TMA·$CoCl_4$ which has the first four modulated phases characterized by wave vectors and space groups $\frac{1}{5}+\delta$(incommensurate), $\frac{1}{5}(Pc2_1n)$, $\frac{1}{5}$-δ(incommensurate), and $\frac{1}{6}(P112_1/n)$. The sequences of phase transitions in these crystals can be easily explained by Fig. 5(c) (trajectory 6).

The sequence of phases in TMA·$MnCl_4$ characterized by wave vectors and space groups $\frac{1}{4}-\delta$(incommensurate), $\frac{1}{4}(P12_1/c1)$, and $\frac{1}{6}(P112_1/n)$ is somewhat different from

the above-mentioned sequences.[59] Also, the first two modulated phases in TMA·$NiCl_4$ (Ref. 60) are similar to the first two phases in TMA·$MnCl_4$. The sequences of phase transitions in these crystals can also be explained by Fig. 5(c) (trajectories 7 and 8).

Gesi[61] reviewed the sequences of modulated phases in these crystals and summarized a unified phase diagram for these crystals. The part of Gesi's phase diagram corresponding to the phases mentioned above is very similar to the phase diagram in Fig. 5.

In the crystals *d*-TMA·$ZnCl_4$ and TMA·$FeCl_4$, for small ranges of temperatures, the phase with a wave vector $\frac{3}{14}$ was observed before th phase transition occurs to the $\frac{1}{5}$ or $\frac{1}{6}$ phases.[56,57] In our model, the phase sequence $\frac{1}{4}$, $\frac{3}{14}$, $\frac{1}{5}$, and $\frac{1}{6}$ is possible. We are not able to extract clear information on an experimentally determined space group for this phase from literature.

When the temperature is further lowered, some crystals in this group go through the low-temperature phase-transition sequence $\frac{1}{6}(P112_1/n)$, $\frac{0}{1}(P2_1/c11)$, and $\frac{1}{6}(P2_12_12_1)$.[8,55–60] The phase diagram in Fig. 11 suggests that the $\frac{1}{6}(P112_1/n)$-$\frac{0}{1}(P2_1/c11)$ phase transition is possible in our model. It also suggests that the $\frac{0}{1}(P2_1/c11)$ and $\frac{1}{6}(P2_12_12_1)$ phases have a common phase boundary. However, the phase sequence $\frac{1}{6}(P112_1/n)$, $\frac{0}{1}(P2_1/c11)$, and $\frac{1}{6}(P2_12_12_1)$ would correspond to an unusual trajectory in the phase diagram (see Fig. 11). The existence of the $\frac{0}{1}(P2_1/c11)$ phase is perhaps related to the fact that the Λ_3 dispersion curve should be acoustic. We have not included an acoustic mode in our model.

Recently, mixture compounds in the TMA·MX_4 group have been studied.[62] The phase behavior of these compounds is similar to that discussed above.

TMA·$CuCl_4$ also belongs to this group according to the chemical composition, but the modulation observed in this crystal belongs to the Λ_2 mode,[63,64] which has the phase sequence $\frac{1}{3}(1-\delta)$, $\frac{1}{3}(P2_1/c11)$, and $\frac{1}{2}(P112_1/n)$. This phase behavior can be well explained by Fig. 9(c).

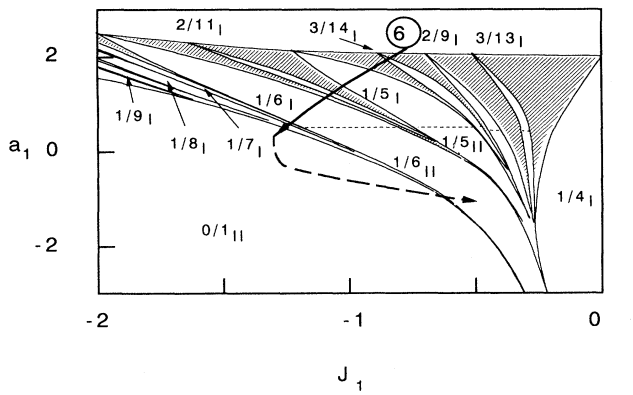

FIG. 11. Phase diagram for given $a_2=0.5$, $J_2=0$, and $\gamma=1$. The phases are labeled by the wave numbers n/m and the space groups in Table II. The integer m is taken from 1–15.

TMA·$CuBr_4$ is isomorphic to TMA·$CuCl_4$ but it is the only member of the A_2BX_4 family that displays modulation in the a^* direction,[65] which is beyond the scope of our model.

V. CONCLUSION

This paper introduces a new type of competing-interaction approach to the problem of finding a universal description of the phases and phase transitions observed experimentally in the A_2BX_4 family of compounds. The basic ideas are to view the structure of these materials as being made up of layers, and to start from an analysis of the symmetry modes of the individual layers. The resulting model displays sequences of modulated phases characterized by both their wave vectors and their space-group symmetries; these sequences correspond to the sequences of phases observed experimentally in the A_2BX_4 family. The free-energy model (2.6) can also be used to explain the phase-transition sequence and the polarization properties observed in betaine calcium chloride dihydrate (BCCD).[66]

Our formulation of the problem contains a number of simplifying assumptions made primarily to reduce the complexity of the problem. For example, we take into consideration only one of each of the Γ_2 and Γ_3 modes, and we make no attempt to correctly model the acoustic branch of Λ_3 symmetry of the phonon spectrum. Also, we consider only nearest-neighbor interlayer interactions, and these only in the quadratic terms of our model free energy. In spite of these simplifications, the observed phase behavior of the A_2BX_4 family, which is discussed in detail in Sec. IV above, is well accounted for by our model. The one exception to this generally good agreement between theory and experiment is the difficulty we have in accounting for the low-temperature sequences of phase transitions from wave vector $\frac{1}{6}$ to 0 to $\frac{1}{6}$ which occur in some of the TMA compounds; this difficulty is possibly due to our inadequate modeling of the Λ_3 acoustic phonon modes.

ACKNOWLEDGMENTS

We acknowledge support from the Natural Sciences and Engineering Research Council of Canada.

APPENDIX A: THE ω_--ONLY MODE

Just below the normal-incommensurate phase transition, only one mode, i.e., the ω_- mode, is stable. We then have, from Sec. II C,

$$f_2=\sum_k \omega_-^2(k)|\Psi_k^-|^2 , \tag{A1}$$

with

$$\bar{v}_k=\alpha_k\Psi_k^-, \quad \bar{w}_k=\beta_k\Psi_k^- . \tag{A2}$$

It is also interesting to transform the quadratic term of the free energy (A1) back to a real-space representation. Introducing a real-space variable for each layer

$$\phi_l = \sum_k e^{iklc'} i\Psi_k^- \ , \tag{A3}$$

we have for the quadratic term per layer

$$f_2 = \sum_l \sum_{l'} \phi_l \phi_{l+l'} \bar{J}_{l'} \ , \tag{A4}$$

with the effective force constant of interaction between layers that are l layers apart,

$$\bar{J}_l = \sum_k e^{iklc'} \omega_-^2(k) \ . \tag{A5}$$

One can generally prove that $\bar{J}_{-l} = \bar{J}_l$. When $l \gg 1$, one can also show that $\bar{J}_l \sim l^{-2}$. The effective interactions are nonlocal now, but the force constant decays fast when l increases, thus the effective interactions are short ranged. If the variable ϕ_l is used, the fourth-order terms in (2.6) can be shown to have a nonlocal form also.

The free energy (A4) can be compared with the Janssen-Tjon model[19] (also called the frustrated ϕ^4 model):

$$F_{\rm JT} = \sum_l \left[\frac{A}{2} \phi_l^2 + \frac{B}{4} \phi_l^4 \right] + \sum_l (C \phi_l \phi_{l+1} + D \phi_l \phi_{l+2}) \ . \tag{A6}$$

There are three major differences. First, the effective long-range interlayer interactions (A5) exist in our model as a result of diagonalizing the phenomenological dynamic matrix for the quadratic term, although we only started with the nearest-neighbor interlayer interaction. Second, our model contains a nonlocal fourth-order term, which is absent in both the Janssen-Tjon model and the mean-field ANNNI model. Third, the variable ϕ_l is not a single-layer variable. The relationship between variables v_l and w_l and ϕ_l can be shown to be

$$v_l = -i \sum_{l'} \phi_{l'} \bar{\alpha}_{l-l'}, \quad w_l = \sum_{l'} \phi_{l'} \bar{\beta}_{l-l'} \ , \tag{A7}$$

where $\bar{\alpha}_l$ and $\bar{\beta}_l$ are the Fourier transforms of the functions α_k and β_k. Note the nonlocal relation between (v_l, w_l) and ϕ_l. The variables (v_l, w_l) represent displacements on layer l; ϕ_l represents a displacement on and in the neighborhood of the layer l.

APPENDIX B: SUPERSPACE SYMMETRY FOR THE INCOMMENSURATE PHASES IN THE A_2BX_4 FAMILY

In this appendix, we deduce the superspace group for the incommensurate phases in the A_2BX_4 family. We assume that the incommensurate phases can be represented by a single harmonic modulation function and that the ω_--only mode is valid throughout the range of the incommensurate phases. The first assumption is a good approximation near the normal-incommensurate transition point. For the purpose of characterizing the symmetry of the incommensurate phases, this simple assumption should be adequate. The second assumption is based on the fact that at a lower temperature when phase transition from the incommensurate phases to commensurate phases occurs, the commensurate phases have the ω_--only mode in the A_2BX_4 family.

Using Eqs. (2.5), (2.8), and (A2), we can show that the displacements of the ions in layer l are represented by

$$u_l(\Delta) = c_1 \cos(kc'l + \Delta) e_l(\Gamma_2) + c_2 \sin(kc'l + \Delta) e_l(\Gamma_3) \ , \tag{B1}$$

where Δ is the phase of the variable Ψ_k in (A2) and c_1 and c_2 are two constants. For a Λ_2-mode incommensurate state with wave vector $\mathbf{k}_r = \kappa \mathbf{c}^*$ in a reduced-zone scheme, $k = \frac{1}{2}(1-\kappa)c'^*$, and Eq. (B1) becomes

$$u_l(\Delta) = c_1(-1)^l \cos(\kappa \pi l - \Delta) e_l(\Gamma_2) + c_2(-1)^{l+1} \sin(\kappa \pi l - \Delta) e_l(\Gamma_3) \ . \tag{B2}$$

The positions of the ions as defined by Eq. (B2) depend on the phase Δ, which can be chosen to have any value, yet not change the free energy. One can then define a four-dimensional superspace structure for the positions of the ions by the coordinates x, y, z, and Δ. The function (B2) describes a "supercrystal" in superspace. The physical displacements can be obtained by a constant-Δ section of the superspace.[27]

A vector in superspace is defined by

$$r = \begin{bmatrix} \mathbf{r} \\ \Delta \end{bmatrix} \ , \tag{B3}$$

where $\mathbf{r}$ represents a usual three-dimensional vector. The incommensurate crystal is periodic in superspace. For incommensurate states of the Λ_2 mode in the A_2BX_4 family, the superspace Bravais lattice translation vectors are

$$A_1 = \begin{bmatrix} a \\ 0 \\ 0 \\ 0 \end{bmatrix}, \quad A_2 = \begin{bmatrix} 0 \\ b \\ 0 \\ 0 \end{bmatrix} \ , \qquad A_3 = \begin{bmatrix} 0 \\ 0 \\ c \\ 2\pi\kappa \end{bmatrix}, \quad A_4 = \begin{bmatrix} 0 \\ 0 \\ 0 \\ 2\pi \end{bmatrix} \ . \tag{B4}$$

The superspace transformation $g = [S \mid W]$ are defined to take one superspace vector r into another, r', where

$$r' \equiv gr = [S \mid W] r = Sr + W \ , \tag{B5}$$

and S denotes a superspace point-group operation defined by

$$Sr = \begin{bmatrix} \hat{S}\mathbf{r} \\ S_\Delta \Delta \end{bmatrix} \ . \tag{B6}$$

Here $\hat{S}$ denotes a physical space point-group operation, and S_Δ denotes a point-group operation on the Δ coordinate which transforms like the z coordinate in physical space under $\hat{S}$.

Using these defintions we can show that for the Λ_2-mode incommensurate phases in the A_2Bx_4 family, the

superspace group $P_{ss\bar{1}}^{Pcmn}$ is valid, which contains the generators

$$[\sigma_x|\tfrac{1}{2}A_1+\tfrac{1}{2}A_3+\tfrac{1}{2}A_4]\ ,$$
$$[\sigma_y|\tfrac{1}{2}A_2+\tfrac{1}{2}A_4]\ , \tag{B7}$$
$$[\sigma_z|\tfrac{1}{2}A_1+\tfrac{1}{2}A_2+\tfrac{1}{2}A_3]\ ,$$

and the translational-group generators (B4).

For a Λ_3 mode with a reduced-zone modulation wave vector $\mathbf{k}_r=\kappa\mathbf{c}$ *, Eq. (B1) becomes

$$u_l(\Delta)=c_1\cos(\kappa\pi l+\Delta)e_l(\Gamma_2)+c_2\sin(\kappa\pi l+\Delta)e_l(\Gamma_3)\ . \tag{B8}$$

The unit vectors are

$$A_1=\begin{bmatrix}a\\0\\0\\0\end{bmatrix},\quad A_2=\begin{bmatrix}0\\b\\0\\0\end{bmatrix},$$
$$A_3=\begin{bmatrix}0\\0\\c\\-2\pi\kappa\end{bmatrix},\quad A_4=\begin{bmatrix}0\\0\\0\\2\pi\end{bmatrix}. \tag{B9}$$

The superspace group is $p_{1s\bar{1}}^{Pcmn}$, which contains generators

$$[\sigma_x|\tfrac{1}{2}A_1+\tfrac{1}{2}A_3]\ ,$$
$$[\sigma_y|\tfrac{1}{2}A_2+\tfrac{1}{2}A_4]\ , \tag{B10}$$
$$[\sigma_z|\tfrac{1}{2}A_1+\tfrac{1}{2}A_2+\tfrac{1}{2}A_3+\tfrac{1}{2}A_4]\ ,$$

and the translational-group generators (B9).

*Present address: Xerox Research Centre of Canada, 2660 Speakman Drive, Mississauga, Ontario, Canada L5K 2L1.

[1]J. D. Axe, in *Incommensurate Phases in Dielectrics,* edited by R. Blinc and A. P. Levanyuk (North-Holland, Amsterdam, 1986), Vol. 2.
[2]H. Z. Cummins, Phys. Rep. **185**, 211 (1990).
[3]M. Iizumi, J. D. Axe, G. Shirane, and K. Shimaoka, Phys. Rev. B **15**, 4392 (1977), and references therein.
[4]S. Kudo, Jpn. J. Appl. Phys. **21**, 255 (1982).
[5]N. Yamada and T. Ikeda, J. Phys. Soc. Jpn. **53**, 2555 (1984); N. Yamada, Y. Ono, and T. Ikeda, *ibid.* **53**, 2565 (1984).
[6]C. J. de Pater and C. van Dijk, Phys. Rev. B **18**, 1281 (1978); C. J. de Pater, J. D. Axe, and R. Currat, *ibid.* **19**, 4684 (1979).
[7]A. C. R. Hogervorst and R. B. Helmholdt, Acta. Crystallogr. B **44**, 120 (1988).
[8]K. Hasebe, H. Mashiyama, and S. Tanisaki, J. Phys. Soc. Jpn. Lett. **49**, 1633 (1980); J. Phys. Soc. Jpn. **51**, 2049 (1982).
[9]G. Marion, J. Phys. (Paris) **42**, 469 (1981).
[10]E. Fjaer, R. A. Cowley, and T. W. Ryan, J. Phys. C **18**, L41 (1985).
[11]*Incommensurate Phases in Dielectrics,* edited by R. Blinc and A. P. Levanyuk (North-Holland, Amsterdam, 1986), Vols. 1 and 2.
[12]Y. Ishibashi, in *Incommensurate Phases in Dielectrics,* Ref. 11, Vol. 2.
[13]H. Mashiyama, J. Phys. Soc. Jpn. **49**, 2270 (1980).
[14]G. Marion, R. Almairac, M. Ribet, U. Steigenberger, and C. Vettier, J. Phys. (Paris) **45**, 929 (1984).
[15]K. Parlinski and F. Dénoyer, J. Phys. C **18**, 293 (1985).
[16]Y. Yamada and N. Hamaya, J. Phys. Soc. Jpn. **52**, 3466 (1983).
[17]P. Bak and J. von Boehm, Phys. Rev. B **21**, 5297 (1980). For recent reviews, see W. Selke, Phys. Rep. **170**, 213 (1988); J. Yeomans, in Vol. 41 of *Solid State Physics,* edited by H. Ehrenreich and D. Turnbull (Academic, Orlando, 1988).
[18]T. Janssen, Ferroelectrics **66**, 203 (1986).
[19]T. Janssen and J. A. Tjon, Phys. Rev. B **24**, 2245 (1981); **25**, 3767 (1982); T. Janssen, in *Incommensurate Phases in Dielectrics,* Ref. 11, Vol. 1.
[20]I. E. Dzyaloshinskii, Zh. Eksp. Teor. Fiz. **46**, 1420 (1964).
[21]J. D. Axe, J. Harada, and G. Shirane, Phys. Rev. B **1**, 1227 (1970).
[22]P. Bak and V. J. Emery, Phys. Rev. Lett. **36**, 978 (1976).
[23]A. P. Levanyuk and D. G. Sannikov, Fiz. Tverd. Tela. (Leningrad) **18**, 423 (1976); **18**, 1927 (1976).
[24]V. Heine and J. D. C. McConnell, Phys. Rev. Lett. **46**, 1092 (1981); J. Phys. C **17**, 1199 (1984).
[25]Z. Y. Chen and W. B. Walker, Phys. Rev. Lett. **65**, 1223 (1990).
[26]F. Axel and S. Aubry, J. Phys. C **14**, 5433 (1981).
[27]P. M. de Wolff, T. Acta Crystallogr. A **30**, 777 (1977); P. M. de Wolff, T. Janssen, and A. Janner, *ibid.* **37**, 625 (1981); A. Janner and T. Janssen, Phys. Rev. B **15**, 643 (1977).
[28]For general references of the materials mentioned in this paper, please refer to Ref. 2. Here we only refer to experiments that determine structures of the crystals in the A_2BX_4 family.
[29]M. Quilichini, P. Bernede, J. Lefebvre, and P. Schweiss, J. Phys. Condens. Matter **2**, 4543 (1990).
[30]K. Gesi and M. Iizumi, J. Phys. Soc. Jpn. **53**, 4271 (1984).
[31]H. Mashiyama and H. Kasatani, J. Phys. Soc. Jpn. **56**, 3347 (1987).
[32]K. Gesi and M. Iizumi, J. Phys. Soc. Jpn. Lett. **46**, 697 (1979).
[33]M. Quilichini and J. Pannetier, Acta Crystallogr. B **39**, 657 (1983).
[34]K. Itoh, A. Hinasada, M. Daiki, A. Ando, and E. Nakamura, Ferroelectrics **66**, 287 (1986).
[35]A. Hedoux, D. Grebille, J. Jaud, and G. Godefroy, Acta Crystallogr. B **45**, 370 (1989).
[36]H. Kasano, H. Mashiyama, K. Gesi, and K. Hasebe, J. Phys. Soc. Jpn. **56**, 831 (1987).
[37]B. W. von Beast, A. Janner, and R. Blinc, J. Phys. C **16**, 5409 (1983).
[38]H. Mashiyama, S. Tanisaki, and K. Hamano. J. Phys. Soc. Jpn. **50**, 2139 (1981).
[39]J. Randa, Phys. Rev. B **32**, 413 (1985).
[40]T. Ueda, S. Iida, and H. Terauchi, J. Phys. Soc. Jpn. **51**, 3953 (1982).
[41]K. Monoto, T. Atake, B. K. Chaudhuri, and H. Chihara, J. Phys. Soc. Jpn. **52**, 3475 (1983).
[42]S. Plesko, R. Kind, and H. Arend, Ferroelectrics, **26**, 703 (1980); Phys. Status Solidi A **61**, 87 (1980).
[43]M. Maeda, A. Honda, and N. Yamada, J. Phys. Soc. Jpn. **52**, 3219 (1983).
[44]N. L. Speziali and G. Chapuis, Acta Crystallogr. B **45**, 20

(1989).
[45]S. Plesko, V. Dvorak, R. Kind, and Treindl, Ferroelectrics **36**, 331 (1981).
[46]D. Altermatt, H. Arend, V. Gramlich, A. Niggli, and W. Petter, Acta Crystallogr. B **40**, 347 (1984).
[47]I. A. Belobrova, A. K. Moskalev, N. V. Bizukina, S. V. Milul, and I. P. Aleksandrova, Solid State Commun. **33**, 1101 (1980).
[48]T. Sato, T. Osaga, and Y. Mikita, J. Phys. Soc. Jpn. **52**, 3297 (1983).
[49]H. Matsunaga, J. Phys. Soc. Jpn. **51**, 864 (1982); **51**, 873 (1982).
[50]J. Warczewski, H. Broda, and D. Kucharczyk, Phase Transition **2**, 131 (1981).
[51]T. Sato, M. Endo, T. Osaka, and Y. Makita, J. Phys. Soc. Jpn. **51**, 3411 (1982); T. Sato, T. Osaka, and Y. Makita, *ibid.* **53**, 1907 (1984).
[52]M. Iizumi and K. Gesi, Solid State Commun. **22**, 37 (1977).
[53]N. Yamada and T. Ikeda, Jpn. J. Appl. Phys. **24**, Suppl. 2, 766 (1985); N. Yamada, T. Ozawa, and S. Kawano. Ferroelectrics **64**, 127 (1985).
[54]G. Madariaga, F. J. Zuñiga, J. M. Pérez-Mato, and M. J. Tello, Acta Crystallogr. B **43**, 356 (1987).
[55]S. Tanisaki and H. Mashiyama, J. Phys. Soc. Jpn. Lett. **48**, 339 (1980).
[56]H. Mashiyama and S. Tanisaki, J. Phys. C **15**, L455 (1982).
[57]G. Marion, R. Almairac, J. Lefebvre, and M. Ribet, J. Phys. C **14**, 3177 (1981).
[58]M. Iizumi, and K. Gesi, Physica B **120**, 291 (1983).
[59]H. Mashiyama and S. Tanisaki, J. Phys. Soc. Jpn. **50**, 1413 (1981).
[60]H. Kasano and H. Mashiyama, J. Phys. Soc. Jpn. **56**, 4192 (1987).
[61]K. Gesi, J. Phys. Soc. Jpn. **51**, 2532 (1982).
[62]E. Colla, P. Muralt, H. Arend, R. Perret, G. Godefroy, and C. Dumas, Solid State Commun. **52**, 1033 (1984); R. Perret, G. Godefroy, and H. Arend, Jpn. J. Appl. Phys. **24**, Suppl. 24-2, 756 (1985); G. Godefroy, Phase Transitions **14**, 139 (1989).
[63]K. Gesi and M. Iizumi, J. Phys. Soc. Jpn. Lett. **48**, 1775 (1980).
[64]J. Sugiyama, M. Wada, A. Sawada, and Y. Ishibashi, J. Phys. Soc. Jpn. **49**, 1045 (1980).
[65]K. Gesi, J. Phys. Soc. Jpn. **52**, 3322 (1983); Ferroelectrics **66**, 269 (1986).
[66]Z. Y. Chen and M. B. Walker, Phys. Rev. B **43**, 760 (1991).